Supplementary Materials

Passive and morphological properties of the model neurons

To estimate the specific membrane capacitance (C_M), membrane resistivity (R_M) and axial resistivity (R_A) values, experimental data were obtained for a small set of neurons, in which the neuron's active conductances were blocked as completely as possible by addition of the following cocktail of blockers (in mM): 0.001 TTX, 2 4-AP, 10 TEA, 0.1 $CdCl_2$, 1 NiCl2, 5 CsCl, 0.01 CNQX, 0.1 AP-5, and 0.04 picrotoxin. Once immersed in this solution, the responses of the neuron to brief current injections (0.5 msec, +1 and -1.5 nA) were measured. Slices were then immediately fixed overnight in cold, 10% formalin in phosphate buffer, processed using Vector ABC kits (PK-6100, Vector Labs., Burlingame, CA), and recorded neurons reconstructed using Neurolucida (MicroBrightField). The passive responses of recorded neurons were evaluated by peeling the slowest two time constants from the voltage decay following current injection (average of 50-100 trials) following a previously described method (Major et al., 1994). For the morphology #1 used in this study, optimal agreement between simulated and experimental passive voltage responses was attained with the following biophysical parameter values: C_M = 0.024 F/m^2, R_M = 1.47 Ωm^2, R_A = 1.74 Ωm. The same passive biophysical parameter values were applied to all three morphological reconstructions used for model neurons examined in this study. The soma was modeled as a sphere. The axon was adapted from (Shen et al., 1999), with an initial segment of 20 microns and 3 myelinated internodal segments of 1 mm each separated by two unmyelinated nodes of Ranvier. The myelinated compartments had no active conductances and had the following passive parameter values: C_M = 0.00024 F/m^2, R_M = 10 Ωm^2, R_A = 1.74 Ωm. The 100-fold reduction of capacitance in myelinated axon segments is following previous axonal modeling assuming a wrap with 50 layers of oligodendrocytic membrane (Shen et al., 1999).

Details of the initial parameter tuning

The tuning process proceeded in several stages and involved changes to the following parameters: the

conductance density parameters of all ion channels in the three main functional regions of the model neuron, the time constant of calcium extrusion from the sub-membrane cytoplasm, the time constant of slow inactivation for the fast sodium channel, and the reversal potential of the passive leak conductance. For each parameter combination, the performance of the model neuron was compared to the electrophysiology template data with respect to the following characteristics: the spontaneous spike rate, the frequency-current response curve for somatic current injections ranging from -200 to +500 pA, spike frequency accommodation during the same current injection stimuli, the spike rate immediately following the cessation of each current injection stimulus, the rate and magnitude of decline in the spike peak amplitude at high firing rates, the presence of depolarization block with large excitatory current stimuli, the ability of the model neuron to recover from depolarization block, and the precise shapes of action potentials and their after-hyperpolarizations. For each parameter combination, error terms were calculated for these characteristics and then combined to generate a weighted sum total error term. The data from the parameter combinations that resulted in the lowest total error were visually inspected, and those combinations judged to provide the best matches to the electrophysiology data were selected as starting points for the next round of tuning. The relative weights of the error measures were adjusted manually during the process to obtain what were considered to be the model parameters exhibiting best qualitative fits. This process resulted in the following model maximal conductance parameters (units: $S/m^{2)}$: NaF=500, NaP=1, Kv2=1, Kv3=10, Kv4f=20, KCNQ=2, SK=4, CaHVA=.3, and HCN=1. These nine conductance density parameters formed the basis of conductance density in the entire model. To adapt specific conductances for different functional regions the following multipliers were used: 0.7x NaF/NaP and 16x SK for the soma; 0.7x NaF/NaP, 2x Kv4f, and 0.1x SK for the dendrites; and 40x NaF/NaP, 40x Kv2/Kv3, 40x Kv4f, and 40x KCNQ for the axon. The high sodium and delayed rectifier concentration in the axon was intended to make this region the spike initiation zone of the model.

Details of the Computer Simulations

For each model, four levels of current injection pulses (CIPs), -100, 40, 100, and 200 pA, were applied in a sequence of simulations, resulting in a total of 503,010 output files. Each file contained 1s of CIP period and 1s

of post CIP control to examine the recovery of physiological activity after each CIP level. An additional file for each combination of parameters contained 1s of spontaneous activity preceding CIP application. To save time, the spontaneous period was run first, and the simulation state was saved in a file for simulating each CIP period starting from this saved state. We used the Hines solver in GENESIS, which is stable even for large time steps and presents an efficient implementation of the Crank Nicholson implicit integration method (Bower and Beeman, 1997, chapter 20). The simulation time step used was 10 μs, as any shorter time steps showed nearly identical solutions. Using 10 μs time steps, each simulation of 2s real time took approximately one CPU minute, requiring 6,706 processor-hours for all simulations. The simulations were run on the High-performance Computing Cluster at Emory University (EHPCC) that hosts 64 nodes of each dual 2.1 GHz AMD Opteron 248 processors. The recorded traces occupied 34 gigabytes (GB) of space in raw form, and they were reduced to 6.8 GB when compressed with custom utility Gencompress (http://userwww.service.emory.edu/~cgunay/pandora/) that uses the FLAC (http://flac.sf.net) lossless audio encoder. The calculation of measurements and the generation of the model DB took about 24 hours on a dual processor Opteron workstation.

Miscellaneous Plotting Methods

In all the instantaneous firing rate plots, the rate is calculated from the inverse of the ISI, and drawn between the times of the bordering action potentials. No binning or filtering was used to prevent artifacts.

Finding the Action Potential (AP) Initiation (Threshold) Point

The AP threshold defined the initiation point of an AP, which was used in determining both the AP amplitude and AHP depth. Thus, its accuracy was an important factor. We used a method of finding the maximal curvature in the phase-plane (Sekerli et al., 2004) combined with the more common method of finding the 15 mV/ms threshold crossing of the first voltage derivative (slope). The latter method was consistent in always finding an AP threshold, but usually found a higher voltage level than the visually apparent point. The phase-plane method gave a better estimate; however, it failed for fast rising, high amplitude APs. We combined the two methods such that, if the slope is already above the threshold at the point found by the phase-plane

method (meaning a high-amplitude AP), it fell back to the slope threshold crossing method. The phase-plane method involved looking at the voltage signal in the slope versus voltage plane. This method required taking several differentials of the voltage data, which would amplify any small noise, especially in the experimental data, to cause great errors. Therefore, all data had to be low-pass filtered and treated at several stages. The voltage signal was first smoothed by a median filter of window size six time steps. The first and second order voltage derivatives were estimated with a central difference technique, improving stability of earlier such techniques (Sekerli et al., 2004), accurate to $O(\Delta t^4)$:

$$\mathrm{d}v(k)/\mathrm{d}t = v' = \left(v(k-2) - 8v(k-1) + 8v(k+1) - v(k+2)\right)/12\Delta t \quad ,$$

$$\mathrm{d}^2v(k)/\mathrm{d}t^2 = v'' = \left(v(k-2) - v(k-1) - 8v(k+1) + v(k+2)\right)/6\Delta t^2$$

where Δt is the time step, which was 0.1 ms in our case. The signal in the phase-plane was then interpolated using a piecewise Hermite interpolating polynomial with the "pchip" function in Matlab to have more data points for the algorithm to work, and median filtered with a window size of 10. The maximal curvature was found from peaks of the classical curvature equation, $C(k) = v''(1 + (v')^2)^{-3/2}$, during the rising edge of the AP.

Measures used in the Neuron Distance Metric

For calculating the distance metric, one could use either the full set of 297 measures, or various selected subsets. These subsets also allowed weighting certain measures to customize quality of match according to the neurophysiologist's priorities. Although larger sets of measures gave a more precise description of discrepancies between two neuron representations, they may be biased for features that were redundantly represented by multiple measurements. A good example of this was when the algorithm matched the AP shape features closely, but tolerated mismatches in rate changes versus injected current levels. In this study, we used a set of 29 measures for the algorithm. The measures can be divided into rate, voltage and action potential measures.

1. Firing rate measures:

a. spontaneous rate

b. rate in the initial 100 ms and in the steady-state of the 40, 100, and 200 pA CIP periods

c. rates in the two halves of the recovery period only after the -100 and 100 pA CIPs

d. special measure of spike-frequency adaptation (SFA) based on ratio of firing rates in the first 100ms versus in the steady-state rate in the +100 pA CIP period

2. Membrane voltage measures:

    a. average voltage of the spontaneous firing period

    b. the average of voltage during, and in the recovery after, the +100 pA CIP period

    c. the average, minimum, and the "sag" of voltage in -100pA CIP period

    d. average voltage in the entire recovery period after -100pA CIP

3. Action potential (AP) measures:

    a. average of AP amplitude, base-width, fall time (the base of the AP is determined by the AP threshold point)

    b. average of threshold measurements by the default and slope-crossing methods (see detailed description of finding the AP threshold point)

    c. AHP depth and AHP minimum point time for all APs in the 100 pA CIP period

    d. The envelope change of AP amplitude during the 100 pA CIP period estimated as a single decaying exponential with total voltage change and a time constant

Some measures in this set had special weights. The average voltage, and the "sag" in the -100 pA CIP period, and the average AP amplitude in the 100 pA CIP period had ten times more weight than other measures. We

resorted to this weighting scheme because these few, but physiologically important, characteristics were otherwise discounted among the better represented features, such as the multiple firing rate measures.

Between models, a parameter distance metric can be calculated (Fig. 6A) similar to the measure distance metric. Instead of using actual conductance values which may differ by orders of magnitude (compare NaF=1000 and HVA=0.03), the conductance levels are normalized by converting to enumerated levels before comparison. That is, the four levels of NaF, 125, 250, 500, 1000, are indicated with the levels 1, 2, 3, 4. The parameter distance metric is then calculated as the city block distance between these levels (i.e., the absolute sum of the parameter differences).

Supplementary Figure Legends:

Supp. Figure 1: Distinct bands in the AP amplitude distribution appeared if morphology and NaF conductance parameter were constrained. (Left) The unrestricted AP amplitude distribution with data from all three mophologies pooled together. (Middle) When the mophology parameter is constrained, four peaks appeared in the distribution. (Right) Restricting further by the NaF conductance revealed that the peak corresponded to one of its conductance levels. AP amplitude was measured from spikes during the initial spontaneous firing period.

Supp. Figure 2: Distinct bands in the AP amplitude vs. half-width plane showed interactions between the two measure with changes in conductance density values. All three plots were restricted to the first morphology. (Left) The three NaF values caused distinct bands of AP amplitude in spite of changing background conductances. (Middle) Kv3 had a major effect on AP halfwidth, although with minor overlap when background conductances were varied. (Right) Kv2 had a major effect on AP halfwidth only for its highest value of 10.

Supp. Figure 3: The effect of the CaHVA conductance on the AHP depth measure was modulated by the SK conductance. This modulation is expected because in the model, the CaHVA channel feeds the Ca concentration

that affects the SK channel. The plot shows the average change in AHP depth for changes in CaHVA conductance levels over all fixed combinations of background conductances. Increments of CaHVA from lowest to medium and from medium to high levels are shown with two separate lines. The upwards extending errorbars show the standard deviation of the measurements from a varying number, *n*, of models from which the AHPs were measured. The x-axis shows the modulatory effect of SK on the relationship between CaHVA and AHP depth.

Supp. Figure 4: Variable effects of TTX application on the electrophysiological characteristics of 10 neurons. Each neuron was applied one or more of the TTX concentrations of 7, 10 or 15 nM in succession. The TTX effect shown in neurons 8-10 was in the presence of 100 μM 4AP applied before taking the baseline values for TTX (lines with diamond markers) and these neurons showed slightly different responses to TTX (e.g., AP amplitude, threshold, sag). These neurons were not included in the analysis for Fig. 10. The AP fixed width characteristic reflected the spike width at +10 mV level. The resting and -100 pA potential characteristic were obtained by averaging raw traces without removing spikes. The -100 pA rebound ratio is the firing rate after a hyperpolarizing -100 pA current injection divided by the spontaneous rate. The +100 pA slowdown ratio is the firing rate after a depolarizing +100 pA current injection divided by the spontaneous rate.

Supplementary Tables:

Supp. Table 1: voltage-dependent gates

Channel	Gate	Pwr	Min_{inf}	$V_{0.5inf}$ mV	K_{inf} mV	τ_{min} ms	τ_{max} ms	$V_{0.5\tau}$ mV	$K_{\tau1}$ mV	$K_{\tau2}$ mV
Na_F	m	3	0	-39	5	0.028	0.028	NA	NA	NA
Na_F	h	1	0	-48	-2.8	0.25	4	-43	10	-5
Na_F	s	1	0.15	-40	-5.4	10	1000	-40	18.3	-10
Na_P	m	3	0	-57.7	5.7	0.03	0.146	-42.6	14.4	-14.4
Na_P	h	1	0.154	-57	-4	10	17	-34	26	-31.9
Na_P	s	1	0	-10	-4.9					
K_V2	m	4	0	-33.2	9.1	0.1	30	-33.2	21.7	-13.9
K_V2	h	1	0.2	-20	-10	3400	3400	NA	NA	NA
K_V3	m	4	0	-26	7.8	0.1	14	-26	13	-12
K_V3	h	1	0.6	-20	-10	7	33	0	10	-10

K_V4_{fast}	m	4	0	-49	12.5	0.25	7	-49	29	-29
K_V4_{fast}	h	1	0	-83	-10	7	21	-83	10	-10
K_V4_{slow}	m	4	0	-49	12.5	0.25	7	-49	29	-29
K_V4_{slow}	h	1	0	-83	-10	50	121	-83	10	-10
KCNQ	m	4	0	-61	19.5	6.7	100	-61	35	-25
Ca_{HVA}	m	1	0	-20	7	0.2	0.2	-20	NA	NA
HCN_{fast}	m	1	0	-76.4	-3.3	0	3625	-76.4	6.56	-7.48
HCN_{slow}	m	1	0	-87.5	-4	0	6300	-87.5	8.9	-8.2

Channel	A_α mV^{-1} ms^{-1}	B_α ms^{-1}	K_α mV	A_β mV^{-1} ms^{-1}	B_β ms^{-1}	K_β mV
Na_P	-2.88 X 10^{-6}	-4.9 X 10^{-5}	4.63	6.94 X 10^{-6}	4.47 X 10^{-4}	-2.63

Steady-state equation for all voltage-dependent gates:

$$X_{inf}(V_m) = Min_{inf} + [(1 - Min_{inf}) / (1 + \exp ((V_{0.5inf} - V_m) / K_{inf})]$$

Standard kinetic equation:

$$\tau(V_m) = \tau_{min} + [(\tau_{max} - \tau_{min}) / (\exp ((V_{0.5\tau} - V_m) / K_{\tau 1}) + \exp ((V_{0.5\tau} - V_m) / K_{\tau 2}))]$$

Kinetics for Na_P slow inactivation (s) gate:

$$\alpha(V_m) = [(A_\alpha * V_m) + B_\alpha] / [1 - \exp \{ (V_m + (B_\alpha / A_\alpha)) / K_\alpha \}]$$

$$\beta(V_m) = [(A_\beta * V_m) + B_\beta] / [1 - \exp \{ (V_m + (B_\beta / A_\beta)) / K_\beta \}]$$

$$\tau(V_m) = 1 / (\alpha(V_m) + \beta(V_m))$$

For Na_F (fast, transient sodium channels) detailed kinetic data on GP neuron sodium currents were not available, but immunohistochemical studies have demonstrated that multiple sodium channel genes, including $Na_V1.2$, $Na_V1.3$ and $Na_V1.6$, are expressed in GP neurons (Hanson et al., 2004). A very precise model of the $Na_V1.6$ sodium channel has been published (Raman and Bean, 2001; Khaliq et al., 2003), and the NEURON code for

this model was kindly provided to us by Dr. I. Raman, Northwestern University. This model includes state-dependent transitions that cannot be reproduced with Hodgkin-Huxley equations; however, we attempted to approximate the activation and fast inactivation characteristics of the model by generating current records with the 13-state model in NEURON, then approximated them with our Hodgkin-Huxley model. The slow inactivation gate was added and parameterized in order to match the frequency-dependent decline in action potential amplitude that was observed during rapid firing in our GP neuron recordings.

The HCN (hyperpolarization-activated, cyclic nucleotide modulated cation channels) were based on the model from Chan et al. (2004), which is a GP-specific adaptation of the model from Wang et al. (2002).

Supp. Table 2: calcium-dependent gate

Channel	Gate	Pwr	$[Ca^{2+}]_{Sat}$ (µM)	EC_{50} (µM)	$K_{\tau\text{-}Ca}$ (ms/µM)	Hill Coeff
SK_{Ca}	m	1	5	0.35	14.4	4.6

SK channel calcium dependence (n = the Hill Coefficient):

$X_{inf}([Ca^{2+}]) = [Ca^{2+}]^n / ([Ca^{2+}]^n + (EC_{50})^n)$

SK channel kinetics:

--for $[Ca^{2+}] < [Ca^{2+}]_{Sat}$, $\tau([Ca^{2+}]) = \tau_{max} - ([Ca^{2+}] * [(\tau_{max} - \tau_{min}) / K_{\tau\text{-}Ca}])$

--for $[Ca^{2+}] >= [Ca^{2+}]_{Sat}$, $\tau([Ca^{2+}]) = \tau_{min}$

Supp. Table 3: Conductance parameters of models in Fig. 3 and Fig. 4A.

Models	NaF	NaP	Kv2	Kv3	Kv4f	KCNQ	SK	CaHVA	HCN	Morph.
t78114 and t50389 (small NaF effect on AP half-width)	-	2	0.1	2	20	0.4	2	3	1	3
t62087 and t2308 (large NaF effect on AP half-width)	-	1	1	10	20	0.4	2	0.3	0.2	1
t116671 and t116698 (Kv3 effect on AP half-width	125	1	0.1	-	10	0.08	2	0.3	1	3
t103720 and t104449 (CaHVA effect on AHP depth)	125	1	1	10	40	0.08	2	-	1	1
t34439 and t34448 (Kv2 effect on AHP)	500	1	-	2	40	0.4	8	0.03	5	2
t19891 and t19892 (NaF effect on AHP depth)	-	0.5	10	10	40	0.4	2	0.03	0.2	2
models t41858 and t42101 (KCNQ effects on rate)	500	2	0.1	50	10	-	2	0.3	0.2	3
models t54787 and t55516 (SK effects on firing rate)	250	1	0.1	10	20	0.4	-	0.3	5	3

Supp. Table 4: The fixed parameters of the model chosen in Fig. 5 for the fine-grade analysis of the NaF versus Kv3 plane.

NaP	Kv2	Kv4f	KCNQ	SK	CaHVA	HCN	morphology
1	1	20	0.4	2	0.3	0.2	2

Supp. Table 5: The normalization coefficients applied to each row of the three-dimensional histogram in Fig. 6A.

Param. Distance	0	1	2	3	4	5	6	7	8	9	10	11	12	13	14
Models in Max. Bin	1	3	20	67	224	458	707	860	728	556	355	164	67	22	4

These coefficients were obtained from the number of models in the largest bin in each corresponding row.

Supp. Table 6: Bidirectional effects of each conductance (and the morphology parameter) on the steady-state firing rate within the +100 pA CIP period.

	Level 1 to 2	Level 2 to 3	Level 3 to 4
NaF	15.2% (-4.00), 21.1%, 63.7% (24.05)	31.9% (-9.29), 20.7%, 47.4% (16.19)	44.7% (-8.90), 20.7%, 34.7% (10.03)
NaP	3.3% (-63.93), 19.2%, 77.5% (11.52)	6.7% (-68.84), 12.0%, 81.3% (12.30)	
NaF-NaP	1.4% (-24.74), 15.5%, 83.1% (23.69)	7.0% (-16.83), 10.6%, 82.4% (14.73)	
Kv2	27.8% (-9.64), 28.8%, 43.4% (9.75)	28.5% (-21.17), 15.7%, 55.8% (20.68)	
Kv3	4.8% (-18.42), 24.9%, 70.3% (14.00)	3.0% (-18.50), 20.8%, 76.1% (18.82)	
Kv4f	57.0% (-6.10), 22.9%, 20.1% (19.64)	61.9% (-8.06), 18.4%, 19.7% (27.70)	
KCNQ	72.1% (-4.14), 24.4%, 3.5% (75.42)	79.1% (-16.19), 10.7%, 10.2% (68.36)	89.5% (-36.39), 6.1%, 4.3% (19.99)
SK	73.7% (-12.30), 22.5%, 3.8% (47.27)	74.8% (-10.11), 22.1%, 3.1% (42.00)	
CaHVA	58.6% (-46.75), 16.9%, 24.5% (51.08)	81.9% (-30.61), 10.2%, 7.9% (31.05)	
HCN	11.3% (-1.02), 42.9%, 45.8% (0.17)	8.7% (-0.81), 34.4%, 56.9% (0.20)	8.1% (-1.09), 28.0%, 63.8% (0.49)
morph	5.0% (-47.99), 24.5%, 70.5% (23.67)	4.8% (-79.89), 13.3%, 81.9% (42.50)	

Several conductance showed bidirectional effects in the histogram of measure change (e.g., in Fig. 4A) for a conductance change to the next level. The table lists percentages of the models that cause rate changes that are less than zero, equal to zero and greater than zero for each conductance level change. The mean values of distribution on either side of the zero bin is given in parenthesis. Rate changes of zero were almost entirely due to models that show depolarization block for both levels of the conductance depicted except in the case of HCN. This was apparent when all depolarization blocked models were excluded from the analysis (not shown).

Supp. Table 7: Conductance combinations of models used for illustrations of specific effects in Figure 10.

Models	NaF	NaP	Kv2	Kv3	Kv4f	KCNQ	SK	CaHVA	HCN	Morph.	Model#
NaF-NaP rate effect	*	*	1	10	20	0.08	4	3	0.04	1	100234
No amplitude change with Kv3	250	0.5	1	*	20	0.4	8	0.03	0.04	3	93647
Amplitude increase with Kv3	125	0.5	1	*	20	2	2	0.03	0.2	2	67990
Doublets	250	1	0.1	*	10	2	4	0.3	5	2	35968
Small NaF effect on AP half-width	*	*	0.1	2	20	0.4	2	3	1	3	78114
Large NaF effect on AP half-width	*	*	1	10	20	0.4	2	0.3	0.2	1	62087

References

Bower JM, Beeman D (1997) The Book of Genesis, 2nd Edition. New York: Springer.

Hanson JE, Smith Y, Jaeger D (2004) Sodium channels and dendritic spike initiation at excitatory synapses in globus pallidus neurons. J Neurosci 24:329-340.

Khaliq ZM, Gouwens NW, Raman IM (2003) The contribution of resurgent sodium current to high-frequency firing in Purkinje neurons: an experimental and modeling study. J Neurosci 23:4899-4912.

Major G, Larkman AU, Jonas P, Sakmann B, Jack JJB (1994) Detailed passive cable models of whole-cell recorded ca3 pyramidal neurons in rat hippocampal slices. J Neurosci 14:4613-4638.

Raman IM, Bean BP (2001) Inactivation and recovery of sodium currents in cerebellar Purkinje neurons: evidence for two mechanisms. Biophys J 80:729-737.

Sekerli M, Del Negro CA, Lee RH, Butera RJ (2004) Estimating action potential thresholds from neuronal time-series: New metrics and evaluation of methodologies. Ieee T Bio-Med Eng 51:1665-1672.

Shen GY, Chen WR, Midtgaard J, Shepherd GM, Hines ML (1999) Computational analysis of action potential initiation in mitral cell soma and dendrites based on dual patch recordings. J Neurophysiol 82:3006-3020.

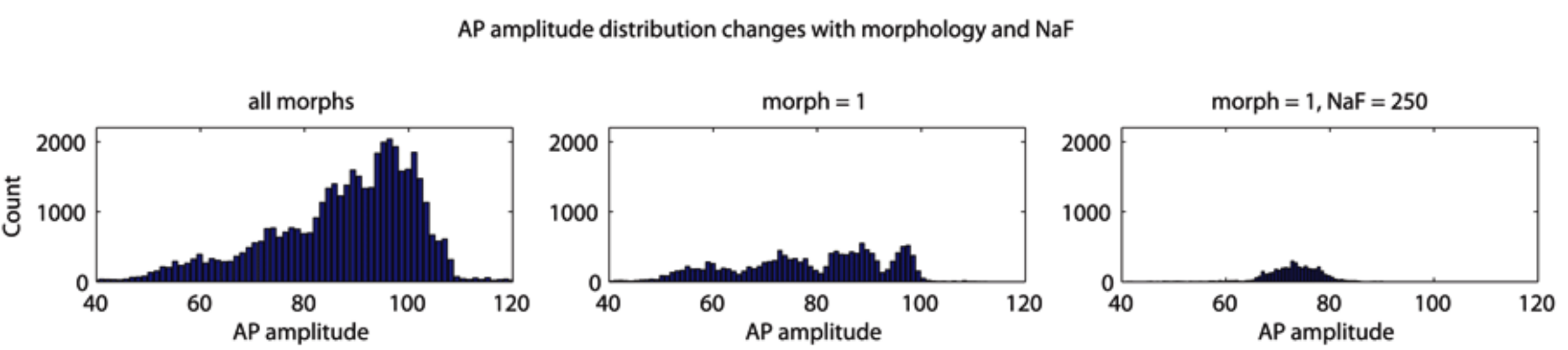
AP amplitude distribution changes with morphology and NaF
all morphs
morph = 1
morph = 1, NaF = 250
Count
2000
1000
0
40
60
80
100
120
AP amplitude

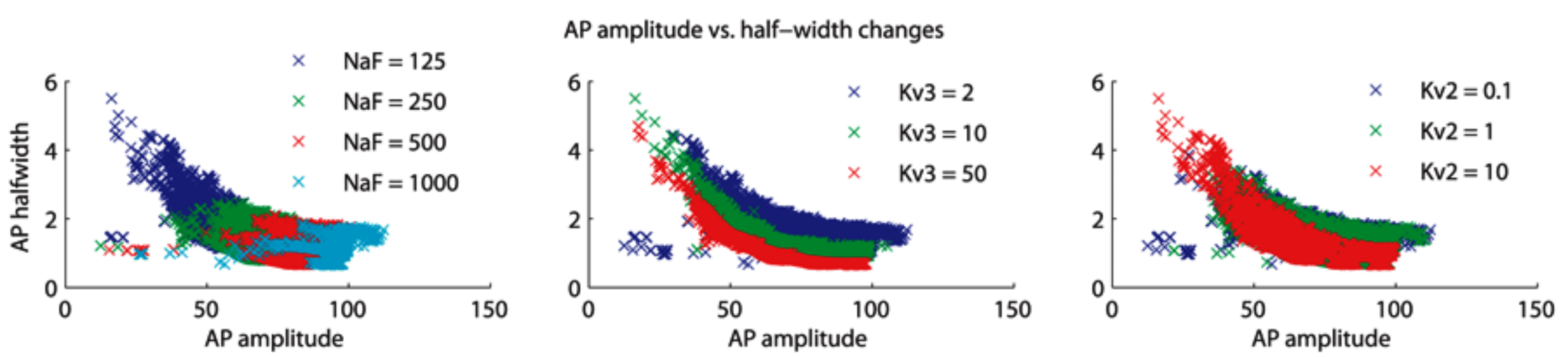
AP amplitude vs. half−width changes
AP halfwidth
AP amplitude
NaF = 125
NaF = 250
NaF = 500
NaF = 1000
Kv3 = 2
Kv3 = 10
Kv3 = 50
Kv2 = 0.1
Kv2 = 1
Kv2 = 10
0
2
4
6
0
50
100
150

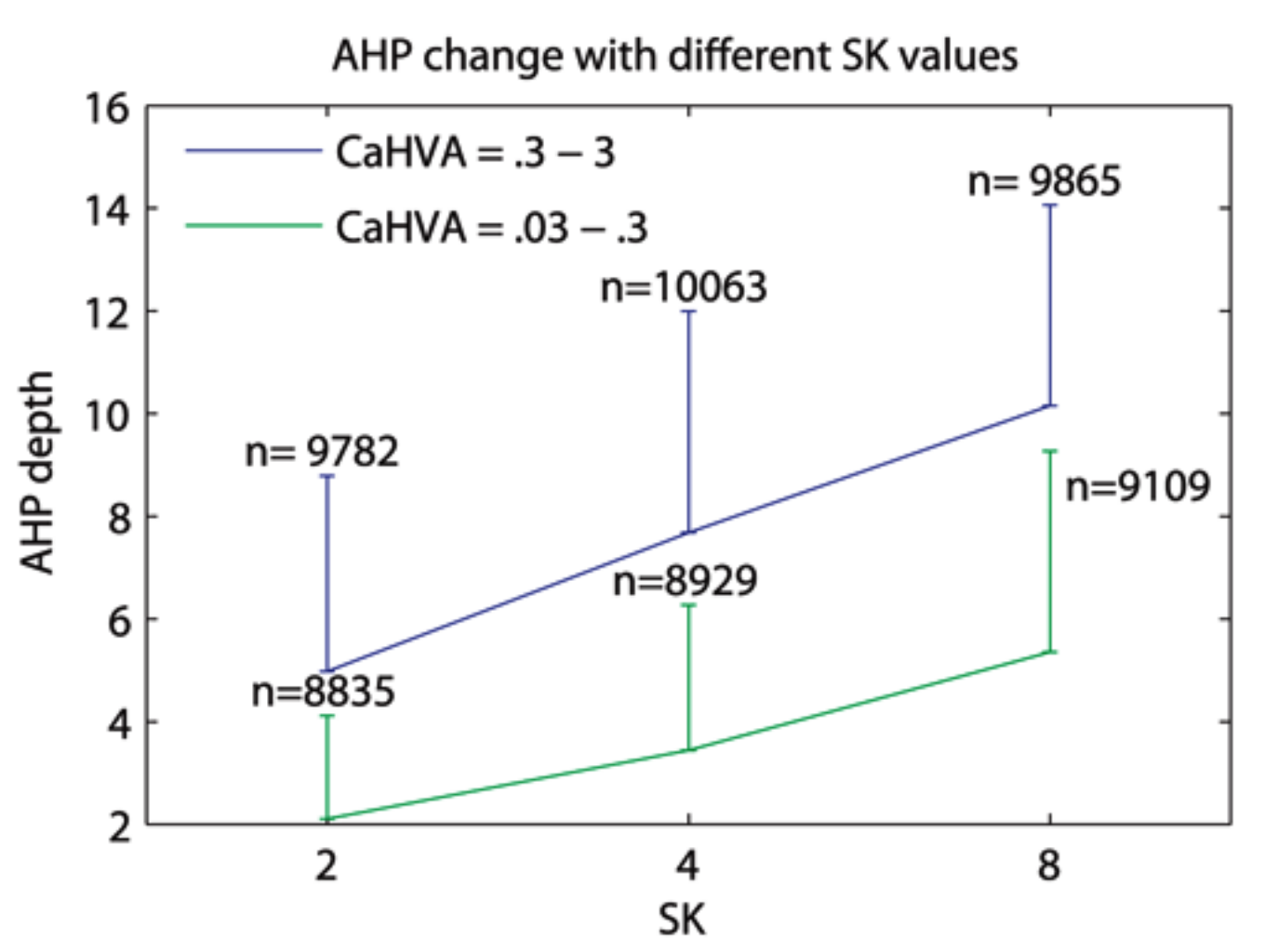
AHP change with different SK values
CaHVA = .3 – 3
CaHVA = .03 – .3
n= 9865
n=10063
n= 9782
n=9109
n=8929
n=8835
AHP depth
SK
16
14
12
10
8
6
4
2
2
4
8

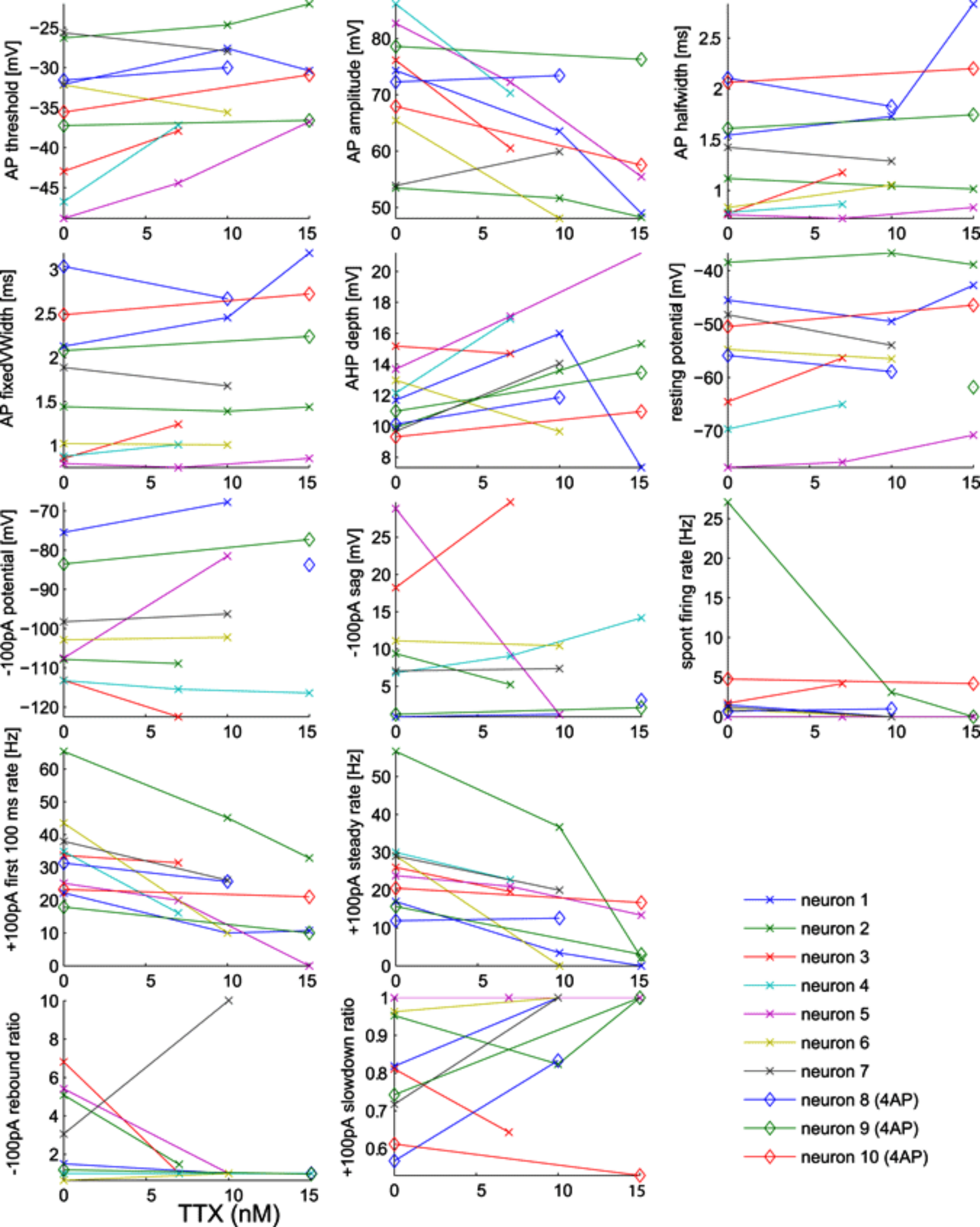
AP threshold [mV]
AP amplitude [mV]
AP halfwidth [ms]
AP fixedVWidth [ms]
AHP depth [mV]
resting potential [mV]
-100pA potential [mV]
-100pA sag [mV]
spont firing rate [Hz]
+100pA first 100 ms rate [Hz]
+100pA steady rate [Hz]
-100pA rebound ratio
+100pA slowdown ratio
TTX (nM)
neuron 1
neuron 2
neuron 3
neuron 4
neuron 5
neuron 6
neuron 7
neuron 8 (4AP)
neuron 9 (4AP)
neuron 10 (4AP)